Proceedings of the
Annual Stability Conference
Structural Stability Research Council
Atlanta, Georgia, April 21-24, 2026

Linear buckling analysis for cable domes

Richard Joao Rosa[1], Krisztian Hincz[2], Sandor Adany[3]

Abstract
In the stability design of slender structures, the critical load is widely employed. Typically, the critical load is interpreted as the load where bifurcation of equilibrium occurs, obtained via linear buckling analysis (LBA). The advantage of LBA is its relative simplicity. In LBA, it is implicitly assumed that the structure is free from mechanisms, and the geometric stiffness is linearly scaled with the loads. However, certain structures are sensitive to deflections, either because small deflections induce significant changes in the internal forces or because the deflections are relatively large. Also, special structures need pretensioning to make them free from mechanisms. In the reported research, cable dome structures are discussed. For the analysis, a MATLAB program has been developed, based on elastic 3D truss bars with large deflection capability. The program can follow the full (occasionally extremely) nonlinear path of the behavior; the potential limit points are surpassed via an arc-length-based solver. The nonlinear solution reveals that although cable domes dominantly carry their load via tensile forces, the presence of compressive elements results in some specific global buckling phenomena. To capture the buckling, LBA cannot be applied directly, since cable domes are pretensioned, and their behavior is inherently nonlinear. Nevertheless, LBA-like procedures are possible; however, the obtained critical load values are dependent on the assumptions introduced. In the paper, a typical cable dome configuration (so-called Geiger-type) is applied to illustrate the nonlinear behavior, to demonstrate the limits, and to discuss the potential applicability of LBA for the stability analysis.

1. Introduction

Cable domes are a prominent member of tensegrity systems in structural engineering, consisting mainly of continuous tension elements with isolated compressive columns, typically arranged in a radial manner. Among the various shapes, one can find the so-called Geiger-type and Levy-type configurations (Fig. 1). The typical elements of the two forms are depicted in Fig. 2. The most obvious advantage of cable domes is the extremely large structural span. Considering the unique properties of tensegrity systems, the behavior is significantly different from that of conventional structures. Geiger domes, for instance, are both statically and kinematically indeterminate. For such a configuration to be load-bearing, the kinematical indeterminacy should fall into the category

[1] PhD Student, Budapest University of Technology and Economics, <rosar@edu.bme.hu>
[2] Associate Professor, Budapest University of Technology and Economics, <hincz.krisztian@emk.bme.hu>
[3] Professor, Budapest University of Technology and Economics, <adany.sandor@emk.bme.com>

of infinitesimal mechanism (in contrast to a finite mechanism), which can be stiffened (in favorable circumstances) with properly selected pretension. Geiger domes, which are the focus of the current study, satisfy this condition and are termed prestressed mechanisms.

The static and kinematic investigation of structures is founded in the literature (for reference, see the work of Pellegrino and Calladine (1986), Pellegrino (1990), and Calladine and Pellegrino (1991)), which can be carried out through the matrix analysis of pin-jointed trusses. The behavior of prestressed mechanisms is inherently nonlinear in nature, as one part of the loads cannot be equilibrated in the initial geometry; hence, they can only be carried through the geometric stiffness, where geometric changes are necessary for load-bearing. Therefore, the geometrical change must be taken into account during the solution. Although geometric nonlinearity can be significant, in some design cases the displacements remain small, and the behavior is practically linear. It is noted that Levy domes (due to the additional cables) are not kinematically indeterminate; hence, they are free from internal mechanisms. This comes with a much larger degree of statical indeterminacy, which makes the structure sensitive to construction imperfections. Finally, a crucial problem arises from the application of cables, where slacking alters the internal structure of the stiffness matrices, leading to significant stiffness loss and/or structural failure.

Figure 1: Real-life structural example: Georgia Dome in Atlanta. The Levy-type configuration was once the largest structural span in the world. The structure was replaced and demolished in 2015. (photo - Birdair)

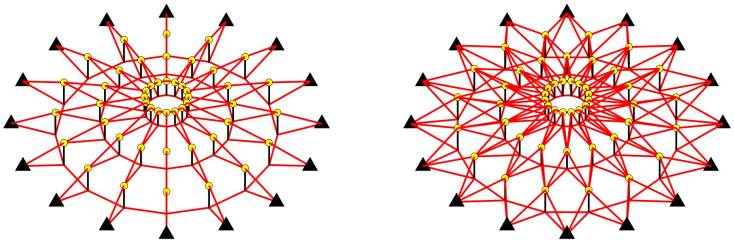

Figure 2: Schematic layout of a Geiger-type (left) and Levy-type (right) cable domes with the identification of the structural member: columns – black, cables – red, hinged supports – black triangles, loaded nodes – yellow dots.

Cable domes have been widely investigated in the literature. However, only a few papers focusing on the global stability analysis are available, e.g., Ahmed and Damatty (2025). Questions can be formulated around the applicability of a simple linear buckling analysis (LBA), the identification of the bifurcation load level, the characterization of the secondary load path, or the existence of limit points. For practical calculations, the application of a conventional LBA preceded by a linear static analysis (LA) is significantly easier to implement and apply than a geometrically nonlinear analysis with or without imperfections (GNA and GNIA, respectively). However, LA and LBA are reasonable only when the geometric nonlinearity is not too significant, a condition that is not necessarily satisfied by cable domes. Another peculiarity of the behavior is due to the presence of internal mechanisms, which result in a singular elastic stiffness matrix in the initial configuration.

Although structures can be stiffened by pretensioning, applying the usual form of the LBA leads to zero eigenvalues. The paper examines two possible forms of the generalized eigenvalue problem (GEVP) for LBA. The main idea is to separate the total stiffness into elastic and different geometric parts. The results are validated against the true bifurcation load level determined by GNA/GNIA.

The report is structured as follows. Section 1 gave a brief introduction to the topic. Section 2 introduces the different LBA and GNIA approaches applicable to prestressed mechanisms. The different formulations are implemented into a solver suitable for the geometrically nonlinear analysis of bar networks written in MATLAB, and introduced briefly in Section 3. Section 4 introduces the investigated structure. Section 5 presents the results of the stability analysis. Finally, Section 6 summarizes the main findings of the paper.

2. LBA for prestressed mechanisms

In structural stability analysis, the calculation is tailored to the static nature of the investigation and the usually linear behavior of engineering structures. The main objective is the identification of the load level at which the system loses its stability. It is evident that this approach inherently assumes small displacements and linear behavior, since the governing equations are linearized around the current equilibrium state. In its most common form, the analysis keeps the elastic part of the stiffness constant and scales the load-dependent geometric part linearly with the load factor, while keeping the geometry-dependent data within the stiffness matrix constant.

For one-parameter loading, the classic form of the GEVP, which gives the condition of static stability loss, is formulated as:

$$\left(\boldsymbol{K_e} + \lambda \boldsymbol{K_g}\right) * \boldsymbol{\Phi} = 0 \tag{1}$$

where $\boldsymbol{K_e}$ is the elastic stiffness matrix, $\boldsymbol{K_g}$ is the geometric part of the stiffness computed from the internal forces, λ is the load factor, and $\boldsymbol{\Phi}$ gives the buckling shape corresponding to the load factor. The geometry is assumed to remain close to the initial configuration; hence, $\boldsymbol{K_e}$ and $\boldsymbol{K_g}$ are determined on the initial geometry, and only the load factor and the internal forces are taken from a preliminary LA. It is noted that every action on the structure, including the constant part of the external loads and pretension, if applied, is scaled linearly in the current form.

In the case of pretensioning, the above form of LBA involves potential issues as follows.

- $\boldsymbol{K_e}$ is singular, which would result in zero eigenvalue(s).
- The initial structure possesses some stiffness from the pretension forces; hence, the initial tangent stiffness matrix is different from $\boldsymbol{K_e}$.
- A single scaling factor is applied for the geometric stiffness, while there are two separate effects: one comes from the external loading, and the other comes from the pretensioning.

Since the pretension is an initial action, it is reasonable not to scale it. One possibility is the separation of the total geometric stiffness into components based on the origin of the internal forces, according to the following form:

$$\left(\left\{\boldsymbol{K_e} + \boldsymbol{K_{g,p}}\right\} + \lambda_l \boldsymbol{K_{g,l}}\right) * \Phi = \left(\boldsymbol{K_{t,ini}} + \lambda_l \boldsymbol{K_{g,l}}\right) * \boldsymbol{\Phi} = 0 \tag{2}$$

where $\boldsymbol{K_e}$ is the elastic part of the total initial tangent stiffness matrix, $\boldsymbol{K_{g,p}}$ is the geometric part of the stiffness computed from the pretension, $\boldsymbol{K_{g,l}}$ is the geometric stiffness calculated from the internal forces induced by the external loads, λ_l is the factor of the external, variable part of the loads, and $\boldsymbol{\Phi}$ gives the buckling shape. In the current formulation, the sum of $\boldsymbol{K_e}$ and $\boldsymbol{K_{g,p}}$ gives the initial tangent stiffness $\boldsymbol{K_{t,ini}}$ of the system. It is mentioned that $\boldsymbol{K_{g,l}}$ is still scaled linearly with the external loads in the current form. Compared to Eq. 1, Eq. 2 provides a possibility to separate the external loads further, e.g., separate the constant (e.g., dead load) part of the external loads and attach them to $\boldsymbol{K_{g,p}}$ (but this is not discussed in this paper)

One question is the separation of the total geometric stiffness into pretension and load-dependent parts. As recalled from Section 1, the investigated structural system is a pin-jointed spatial bar network; therefore, the members are pinned-pinned truss elements (and the structure of the elastic and geometric stiffness matrices is the well-known simple form of this tension-compression element). While the total geometric stiffness can be computed from the internal forces at any loaded configuration, the above formulation requires some specific separation of the internal forces that go into $\boldsymbol{K_{g,p}}$ and $\boldsymbol{K_{g,l}}$, respectively. As a starting point, $\boldsymbol{K_{g,p}}$ can be determined easily in the prestressed but unloaded configuration. After applying any load, the internal forces from the loads are imposed on the initial internal force distribution in a generally nonlinear manner. As a basic idea, the internal forces are separated assuming linearity, in the following form:

$$\boldsymbol{K_{g,p,ij}} = N_{p,ij}\boldsymbol{K_{g,ij}} \tag{3}$$

$$\boldsymbol{K_{g,l,ij}} = \left(N_{l,ij} - N_{p,ij}\right)\boldsymbol{K_{g,ij}} = \Delta N_{ij}\boldsymbol{K_{g,ij}} \tag{4}$$

where $N_{p,ij}$ is the normal force in element ij computed at the prestressed but unloaded structure, $N_{l,ij}$ is the normal force in element ij in the loaded and pretensioned configuration, and $\boldsymbol{K_{g,ij}}$ is the elementary geometric stiffness matrix of the element. In this form, the load-dependent part is computed from the total increment ΔN_{ij} of the normal forces.

It is noted that Eq. 2 was written for a constant pretension. In a more general form, the pretension could also be treated as a variable effect, with the corresponding λ_p scaling factor, leading to a two-parameter GEVP:

$$\left(\boldsymbol{K_e} + \lambda_p\, \boldsymbol{K_{g,p}} + \lambda_{load}\, \boldsymbol{K_{g,l}}\right) * \boldsymbol{\Phi} = 0 \tag{5}$$

In the upcoming investigations, the previously introduced formulations of the GEVP, given by Eqs. 1 and 2, will be examined.

3. Numerical model and applied methodology

The numerical model is constructed from two-node, straight, pin-jointed tension-compression truss elements and tension-only cable elements. For consideration of cable slacking, if needed, the algorithm discretizes the cables using two-node tension-only elements, which can model the curved shape while maintaining a simple linear element formulation. Local buckling is prevented by using a single element per column. The applied material is linearly elastic, compression in cables is prevented by a bilinear material model. The numerical model is based on the direct

stiffness method of pin-jointed space frameworks. The solution of the nonlinear equation system utilizes the Newton-Raphson iteration. Considering the relatively small number of degrees of freedom, it is possible to update the stiffness matrices in every iteration step, ensuring faster convergence. The solutions are obtained through the arc-length method of Crisfield (1981), which enables numerically stable solutions around bifurcations and limit points. Pretension is carried out through the matrix analysis of the equilibrium equations based on Yuan and Dong (2003). The validation of the developed model is based on the work of Pellegrino (1992), which investigated a small-scale Geiger dome. The validation results are presented in Rosa and Hincz (2023) using the dynamic relaxation method for the static analysis of the small-scale model. The current algorithm, based on the matrix displacement method, was compared to the previously validated model.

The flowchart of the investigation is shown in Fig. 3. The calculation starts with the initial geometry definition. Then, the equilibrium matrix of the structure is set up, through which the available self-stress states and the internal mechanisms are determined. The pretension of the structure is selected in the next step with a proper linear combination of the independent self-stress states. The load analysis is carried out in the next step. If the members and the pretension are appropriately selected, the structure satisfies the design criteria (member load-bearing and avoidance of slacking). Determining such a structural configuration may require some iteration. After the pre-sized structural system is available, the nonlinear structural behavior can be investigated by GNA/GNIA. However, applying imperfections (either in the form of imperfect initial geometry or imperfection loads) requires some knowledge about the stability characteristics of the structure. In practice, LBA typically helps identify a proper distribution of imperfections.

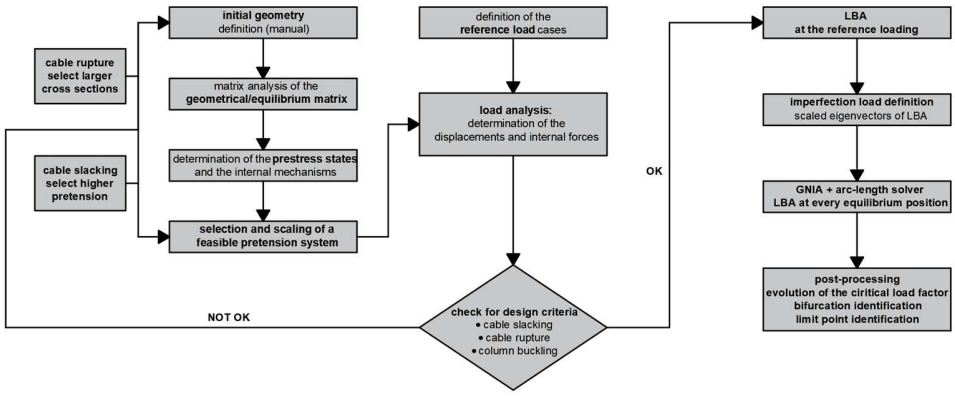

Figure 3: Methodology of simulation from the geometry definition to the post-processing of the results.

It is noted that the application of (global) initial geometric imperfections is not possible due to the pretension, which would pull back the perturbed shape into a “perfect geometry”. Although some modification of the stress-free element lengths might occur, and the new system would slightly differ from the original one, the essence of geometric imperfections – the introduction of initial eccentricities – could not be ensured. However, with the definition of imperfection loads, one can ensure a perturbed initial equilibrium shape, on which the effect of external loads can be superimposed. In the current methodology, imperfection loads are applied. The distributions of these loads are identical to the nodal displacements of the chosen eigenvector of the LBA; this displacement vector is then scaled to get a desired load vector with maximum load intensity (which is otherwise small, compared to the external loads, so it will only cause a small perturbation).

4. Investigated structure

The investigated structure is a Geiger-type cable dome depicted in Fig. 4. The characteristic dimensions and the nodal coordinates of a single radial segment are shown in Fig. 5. The structural span is 50 m. The structure consists of 2 internal hoops and 16 radial segments. The radial segments consist of two radial cables between every neighboring column, connecting the upper node of the outer column with the internal column's endpoints. Lower hoop cables connect the radial segments, ensuring the transmission of forces between them. Regarding the internal closing of the structure, a tensile hoop, a floating column (as a continuation of the radial cables), or a rigid cylindrical truss (which ensures rigid body motion while keeping the modeling with pin-jointed truss elements) can be applied. In the current investigation, a rigid cylindrical truss was employed, primarily to address the issues of the upper hoop cables slackening in case of the conventional tensile hoop. The total number of cables is 128, while the number of columns is 32, respectively

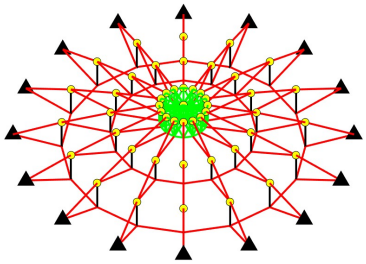

Figure 4: Spatial view of the investigated structure. The colors are depicting: columns – black, cables – red, rigid internal cylinder – green, hinged supports – black triangles, loaded nodes – yellow dots.

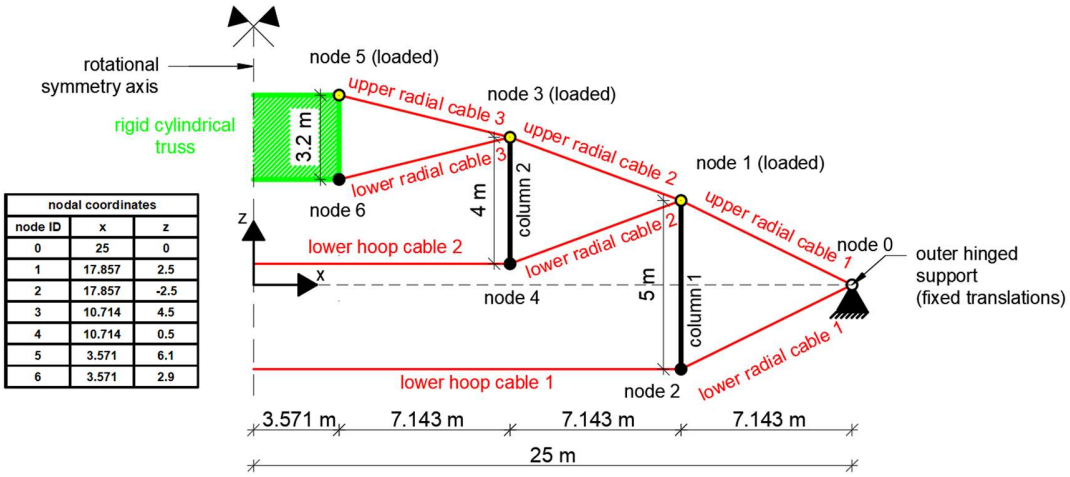

nodal coordinates		
node ID	x	z
0	25	0
1	17.857	2.5
2	17.857	-2.5
3	10.714	4.5
4	10.714	0.5
5	3.571	6.1
6	3.571	2.9

Figure 5: A radial segment with the structural components in the manually defined initial shape of the structure (before pretension). The nodal coordinates of the pretensioned structure differs from the ones depicted in the figure.

The structure is investigated under a total distributed load with a constant intensity of 1 kN/m². The upper nodes are loaded as shown in Figs. 4 and 5. It is noted that partial loads can impose significantly larger structural displacements in cable domes, as they excite the internal mechanisms of the system to a greater extent (however, this is not discussed in the current report).

One comment needs to be mentioned at this point. Typical failure mechanisms of Geiger-type cable domes are (1) cable slacking under large deflections due to the decreasing cable lengths, (2) cable rupture of the overloaded members, (3) local buckling of the columns, and (4) global

buckling of the structure. Cable slacking (1) (typically in the internal zones and the upper cables), although it decreases the global stability significantly, does not lead to global structural failure based on Zhu et al. (2016). Moreover, the slacking can be immediately connected to a global buckling (4), due to the vanishing stabilizing effect that introduces singularity to the tangent stiffness matrix. Local buckling (3) can be treated (prevented with proper sizing) on the element level, although the structural effect of local buckling could be further analyzed in the future.

The current report deals with the global instability phenomenon of cable domes (4). One can ensure that failure types (1) – (3) do not occur along the way by correctly pre-sizing the structural members. Correct cross-sections prevent the element rupture and local buckling, while slacking is prevented by sufficiently large pretension. This calculation requires some iteration; otherwise, the design is straightforward. On the other hand, failure mechanisms (2) and (3) are excluded from the current investigation due to the spatial truss model (without the modeling of bending) and the linear elastic material model. These simplifications enable the isolation of failure type (4).

The structural members were pre-sized under the applied loads, considering the tension resistance of the cables and the buckling loads of the columns. The column sections are circular hollow sections (CHS), while the cross-sectional area of a single high-strength steel cable is 176.31 mm^2. The applied column sections, the cable numbers, the stress-free lengths, and the pretension forces are shown in Tables 1 and 2. Figs. 4 and 5 with Tables 1 and 2 ensures the reproducibility of the results. It is noted that the only purpose of this step was to ensure a reasonable global stiffness.

Table 1: Pre-sized structural members and pretension forces - columns

element name	diameter [mm]	wall thickness [mm]	stress-free length [m]	pretension [kN]
column-1	168.3	4.0	5	-270.4
column-2	106	3.6	4	-108.2

Table 2: Pre-sized structural members and pretension forces - cables

element name	cable number	stress-free length [m]	pretension [kN]
radial-cable-lower-1	9	7.542	819.2
radial-cable-lower-2	4	7.389	401.5
radial-cable-lower-3	2	7.292	197.9
radial-cable-upper-1	8	7.538	818.7
radial-cable-upper-2	4	7.389	401.0
radial-cable-upper-3	2	7.292	197.9
hoop-cable-lower-1	22	6.944	1971.9
hoop-cable-lower-2	10	4.165	991.0

5. Results

Figs. 6 and 7 show the first six buckling modes and the corresponding eigenvalues under total load, determined using Eqs. 1 and 2 in Section 2, respectively. Table 3 gives the tabulated results of the first six non-zero eigenvalues. Zero eigenvalues can occur in the case of Eq. 1, where the constant part of the total stiffness matrix - only coming from the elasticity of the structure - is singular due to the presence of internal mechanisms.

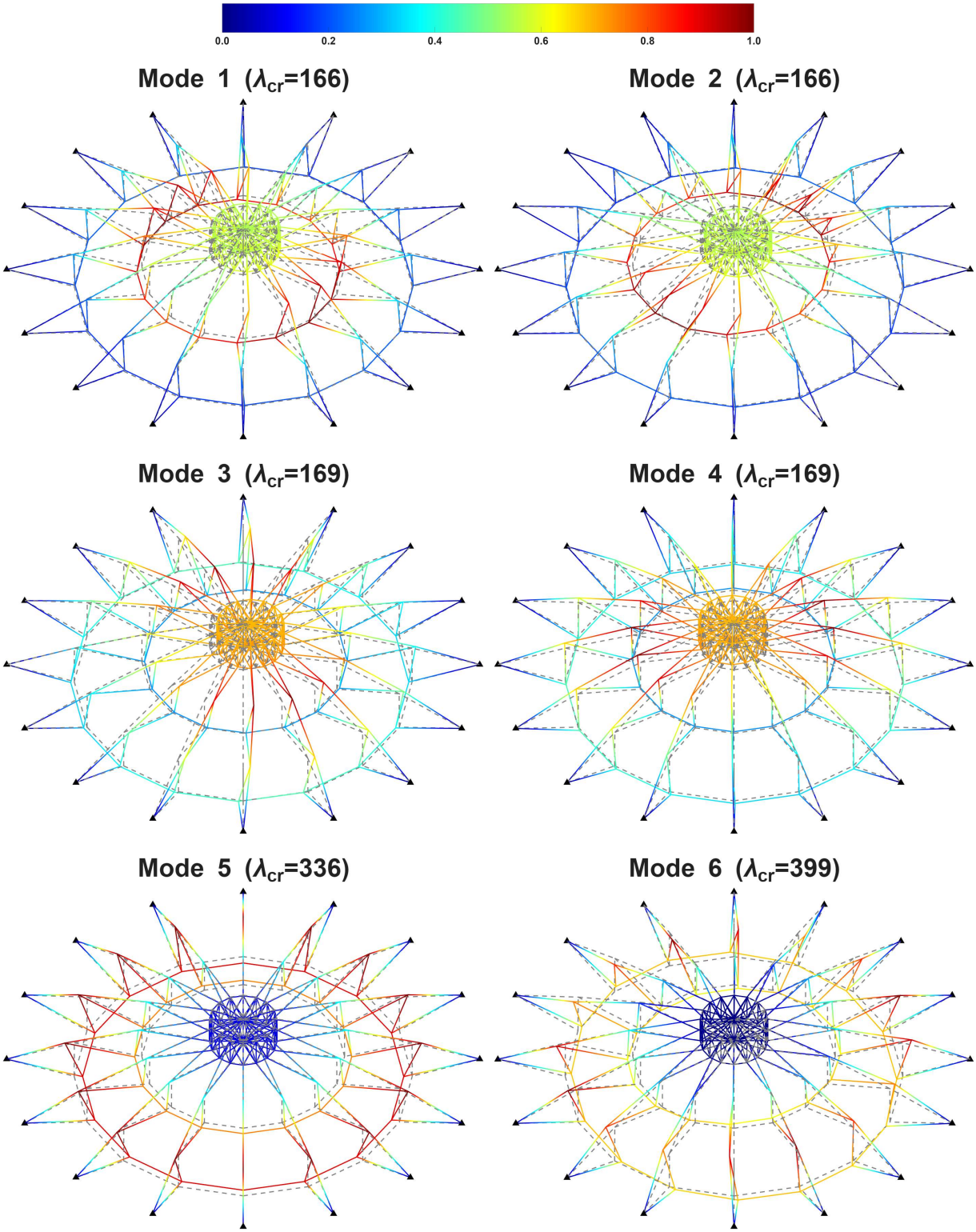

Figure 6: First six eigenmodes and eigenvalues of the Geiger cable dome under total vertical loading determined with the conventional form of the GEVP given by Eq. 1. The figures are colored according to the magnitude of the resultant displacement. The gray dashed line depicts the original shape.

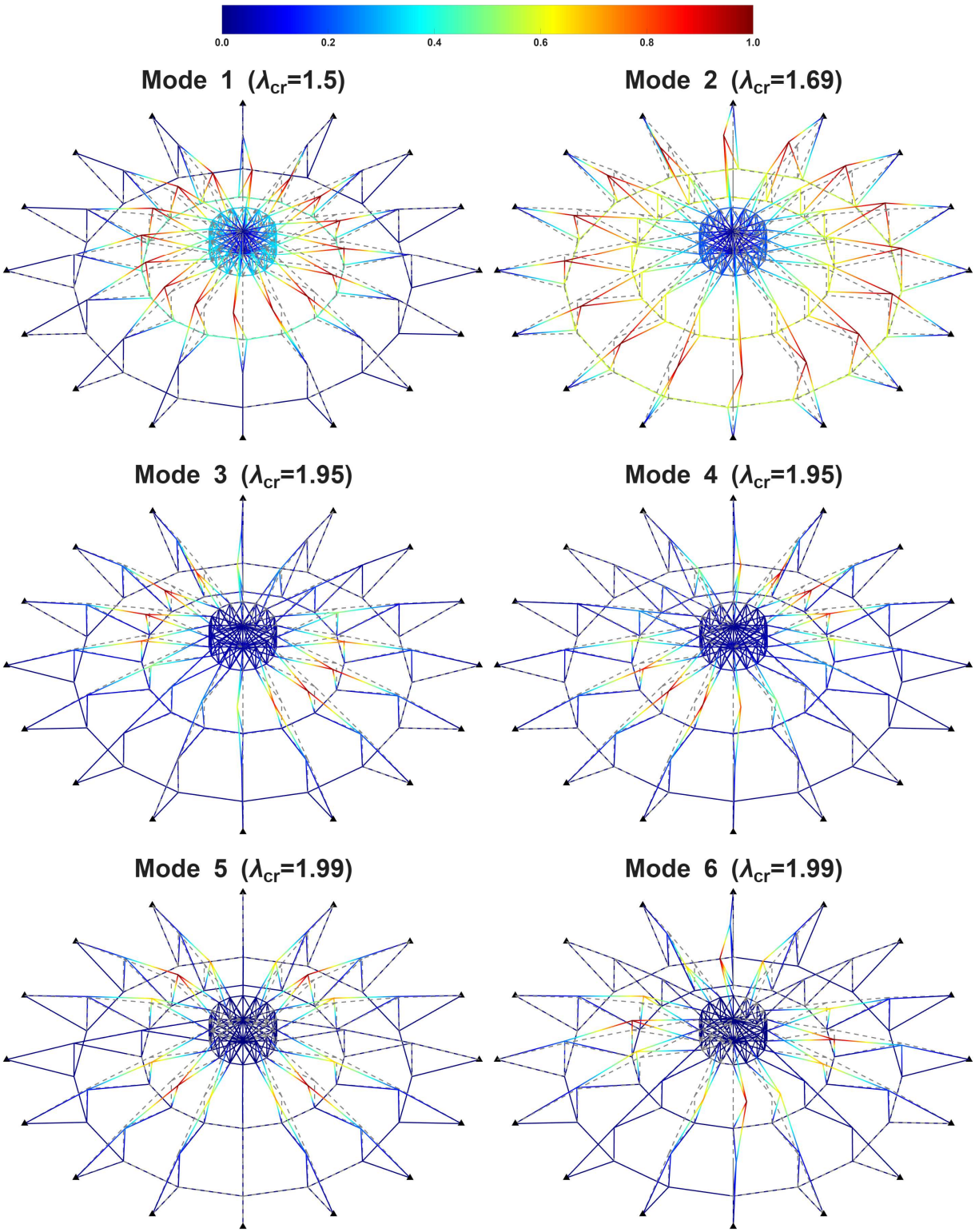

Figure 7: First six eigenmodes and eigenvalues of the Geiger cable dome under total vertical loading determined with the modified form of the GEVP given by Eq. 2. The figures are colored according to the magnitude of the resultant displacement. The gray dashed line depicts the original shape.

Table 3. Characterization of the eigenvalues and eigenvectors.

Formulation of the GEVP		First six nonzero critical load factors and corresponding eigenvectors						Geometric multiplicity of 0 eigenvalue
		Mode #1	Mode #2	Mode #3	Mode #4	Mode #5	Mode #6	
Eq. 1	eigenvalue	166	166	169	169	336	339	81
	characterization of the buckling shape	inner hoop rotation (horizontal axis)	inner hoop rotation (horizontal axis)	inner core horizontal translation	inner core horizontal translation	column rotation in the radial plane	inner/outer hoop ovalization	81
Eq. 2	eigenvalue	1.5	1.69	1.95	1.95	1.99	1.99	0
	characterization of the buckling shape	torsion of inner hoop	torsion of outer hoop	inner hoop translation $sin(\varphi)/cos(\varphi)$	inner hoop translation $sin(\varphi)/cos(\varphi)$	inner hoop translation $sin(2\varphi)/cos(2\varphi)$	inner hoop translation $sin(2\varphi)/cos(2\varphi)$	0

The results of the different GEVPs based on Figs. 6 and 7, and Table 3 are summarized as follows:

- Results of Eq. 1 (conventional LBA – Fig. 6):
  - The 1st and 2nd buckling modes are characterized by the rotation of the inner hoop around two different horizontal axes, resulting in tilted inner columns. The corresponding eigenvalue is a double root of the characteristic equation.
  - The 3rd and 4th buckling shapes, also with a double root, are characterized by the horizontal translation of the rigid cylindrical truss and tilted inner columns.
  - The 5th mode corresponds to the rigid body rotation of the outermost columns (without elastic deformation due to the pinned-pinned model) in the plane of each radial section.
  - Mode 6 is characterized by the deformation/ovalization of the inner and outer hoop.
- Results of Eq. 2 (modified LBA – Fig. 7):
  - The 1st and 2nd buckling modes correspond to the global torsion of the structure. The smaller root belongs to the rigid body rotation of the inner columns, while the second corresponds to the same motion of the outer columns. Examining the distribution of the translations in the tangent direction of hoops along the central angle φ, the translations are constant in modes 1 and 2, respectively.
  - Buckling modes 3-4 and 5-6 belong to two double roots. Translation of the inner column upper nodes in the hoop tangent direction characterizes these shapes. In modes 3-4, the distribution of these translations along φ can be described as $sin(\varphi)$ and $cos(\varphi)$ (columns along a single diameter remain in position in each mode). Similarly, this distribution in modes 5-6 is given by $sin(2\varphi)$ and $cos(2\varphi)$ (columns remain in place along two perpendicular diameters in each mode).
- The conventional form of the GEVP given by Eq. 1 provided critical load factors larger by two orders of magnitude compared to the modified form of Eq. 2.
- The global torsional buckling modes 1-2 of the modified form of Eq. 2 correspond to the typical modes determined by, e.g., Tomka (1997). These modes can be explained by the small geometric stiffness of the upper nodes, where the tension in the radial cables is the primary source of rigidity, which is otherwise small.
- The multiple double roots of the characteristic equations are caused by the circular symmetry of the cable dome.

The following section introduces the load-displacement characteristics of the structure. The simulations were carried out using GNA/GNIA and the arc-length method. The evolution of the smallest critical load factor during the loading of the structure is also examined, providing insight into the effect of geometric nonlinearity. It is noted that the diagrams show the actual load level normalized by a (reference) buckling load $q_{b,ref}$. This buckling load was determined in the equilibrium shape under the reference load intensity of 1.0 kN/m^2. The corresponding load factor is 1.5 (mode 1 of Fig. 7), hence $q_{b,ref}$ = 1.5 kN/m^2. The normalization explains why the load-displacement curves kink around 1.0.

Fig. 8, top left, illustrates the load-displacement curves obtained for the perfect geometry using GNA. The kinks in the diagrams demonstrate the bifurcation of the equilibrium path of the structure. Translations of the inner column upper node (node 3 in Fig. 5) are shown in the vertical direction (red curve – characterizing the global deflection) and in the tangent direction, perpendicular to the plane of the radial segments (blue curve – translation in the principal direction of buckling based on the 1st mode of Fig. 7).

The evolution of the critical load factor based on the modified form of Eq. 2 is illustrated in Fig. 8, top right. The load – vertical displacement curve of node 3 (red curve) is repeated in the figure, and the critical load level (computed from the first eigenvalue of Eq. 2) is plotted against the vertical displacement (black curve). The interpretation of the diagram is as follows: a point on the red curve represents the equilibrium configuration (structural deflection) under the current load level, while the corresponding point on the black curve (with the same displacement on the horizontal axis) shows the buckling load calculated from the LBA (Eq. 2) based on the deformed geometry.

The load-displacement characteristics of the structure are also investigated with and without the consideration of imperfections. Fig. 8, bottom left, depicts the load-displacement diagrams determined with GNA and GNIA. GNA is carried out on the perfect structure combining the arc-length method with mode injection/eigen-shape perturbation at the bifurcation of the equilibrium path. Based on the reasoning of Section 3, geometric imperfections cannot be applied; hence, imperfection loads are used for GNIA. Four different levels of imperfection loads are considered. The distribution of these loads is identical to the eigenvector corresponding to the smallest critical buckling mode of Fig. 7. The maximum entry of each load vector in [N] is depicted in the legend. Comparing the results under different imperfection load magnitudes gives an insight into the imperfection sensitivity of the structure. Finally, Fig. 8, bottom right, shows the evolution of the smallest critical eigenvalue of the tangent stiffness matrix, which characterizes the nature of the equilibrium state at each configuration.

Fig. 9, left, illustrates the typical equilibrium shape of the structure along the secondary branch with global torsional deformation, while the normal forces of each element class (for reference, see Fig. 5) are plotted against the normalized load level in Fig. 9, right. The internal forces are also normalized (with the pretension forces of the elements given in Tables 1 and 2); hence, the diagram illustrates the relative change of the normal forces. Due to the rotational symmetry of the structure and the loading, elements in the same position have identical internal force histories.

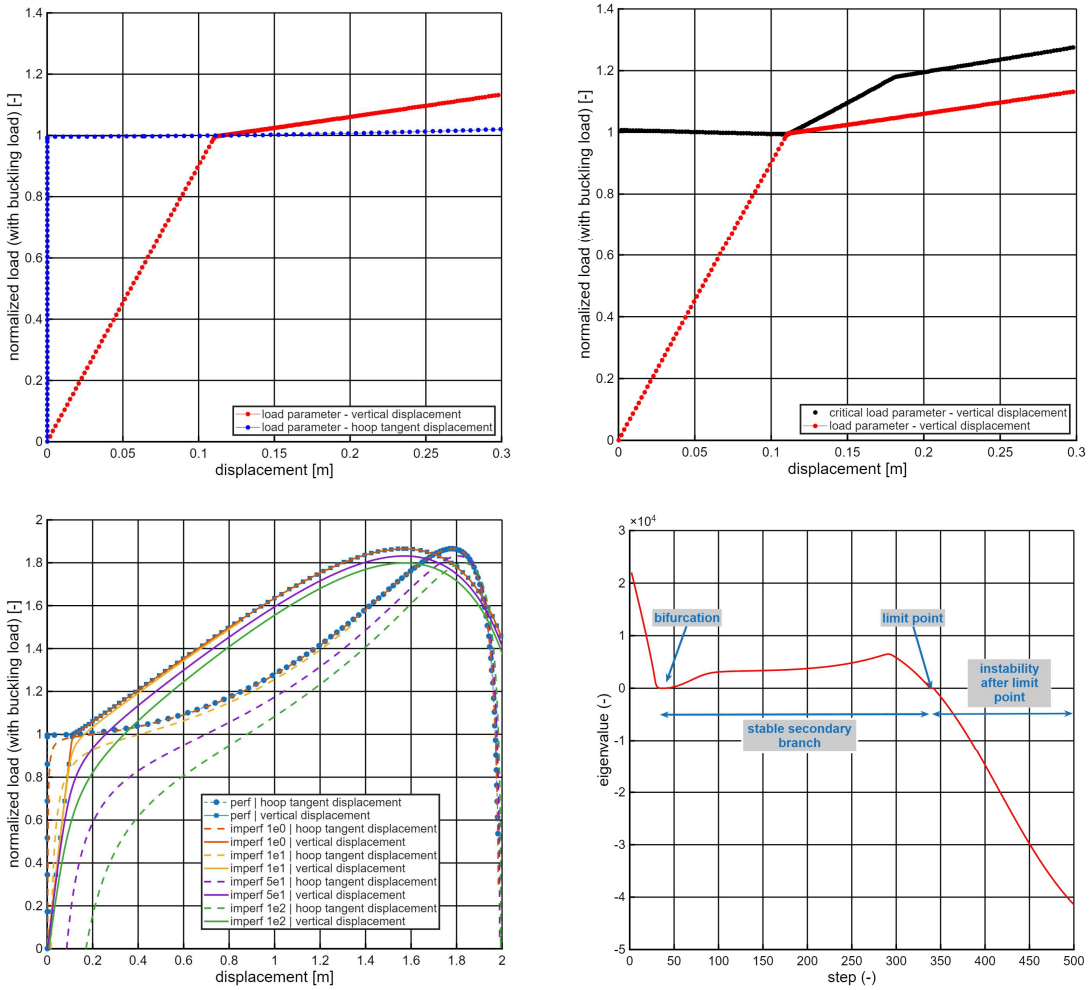

Figure 8: Top left: Load-displacement of node 3 in vertical direction and tangent direction to the hoop (GNA). Top right: Critical load of the deformed structure plotted against the load-induced deflection (GNA + LBA). Bottom left: Load-displacement curves without (GNA) and with (GNIA) different levels of imperfection loads. Bottom: Smallest eigenvalue – load step for the characterization of the stability.

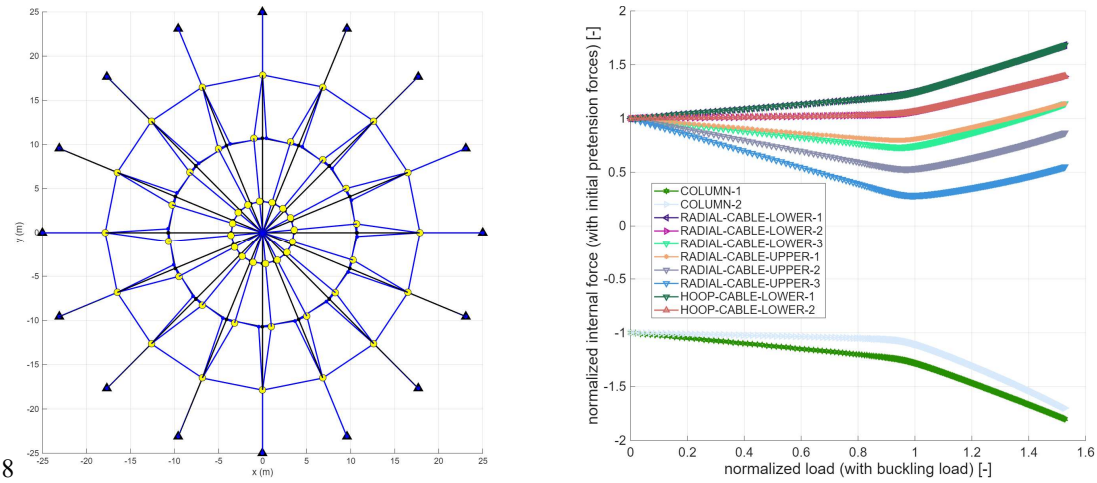

Figure 9: Left: Top view of equilibrium shape along the secondary branch with (global) torsional deformation. Right: Internal forces in the function of the load magnitude (from GNIA with imperf 1e1 from Fig. 8, bottom left).

The following conclusions can be drawn from Figs. 8 and 9:

- Under no/small imperfections (Fig. 8, top left and bottom left), the structure behaves linearly in the initial stage of the loading. This initial linear regime ends with a bifurcation, after which the behavior becomes nonlinear, with an initially increasing and finally decreasing branch, indicating a limit point. Strong nonlinearity is observed only around the limit point.
- Increasing the imperfections (Fig. 8, bottom left) increases the level of nonlinearity, and the sharp change in the load-displacement curve vanishes. The effect of the initial imperfection magnitude is small on the maximal load level given by the limit point (approximately a 5% decrement can be observed).
- Comparing the results of the GNA/GNIA simulations and the LBA of Eqs. 1 and 2, it is evident that the conventional formulation is inadequate. At the same time, the modified form of the LBA provided critical load factors close to the true buckling load. The poor results of Eq. 1 are due to the linear scaling of the self-stress state, which is a constant initial effect.
- Applying LBA (Fig. 8, top right) in the initial, linear regime provides a good approximation of the critical load level at any equilibrium state, independent of the magnitude of the external loads. The repeated solution of the GEVP reveals that the change in the critical load level is small (less than 2% in the current example), and the value decreases with increasing load level; hence, the prebuckling deflections cause a slight negative (and practically negligible) effect on the buckling load.
- The secondary branch (Fig. 8, bottom right) indicates stable behavior, which is justified through the sign-check of the smallest eigenvalue of the tangent stiffness matrix. Except in the vicinity of the bifurcation, the smallest eigenvalue is positive until the limit point.
- The equilibrium shape in the secondary branch (Fig. 9, left) is subjected to large torsional deformation between the bifurcation and the limit point.
- Stability along the secondary branch is ensured by the increasing cable forces, which are generated by the rotation of the buckled columns. In the mechanism, the internal forces of certain cables are decreasing along the primary branch (Fig. 9, right – upper radial cables). The upper nodes, initially stabilized by these cables, lose their stability, and global torsional buckling develops. These unstable upper nodes regain stability through the increasing cable forces caused by their elongation during the rotational movement of the columns. This stabilizing effect in the initial, increasing part of the secondary branch is larger in magnitude than the destabilizing effect of the rotated columns' compressive forces. There is a well-defined qualitative change in the behavior at the limit point, where the cable force is no longer able to compensate for the out-of-plane forces of the buckled columns.
- The regained stability can be explained with the statical indeterminacy of the system, which ensures redundancy and mobilized load-bearing capacity after the bifurcation. This phenomenon is similar to a simple plate buckling.
- The first bifurcation point, due to the redundancy hidden in the statical indeterminacy, does not mean global failure. The limit point ensures an approximately 80% increase in load-bearing capacity, although at the expense of significant structural deformation. It has to be noted, though, that the column forces (Fig. 9, right) are increasing intensively in the secondary branch; hence, their local buckling can limit this load-bearing capacity. However, this local buckling can be prevented with proper member sizing.

6. Conclusions

The report introduced the results of a preliminary study on the global stability of cable domes. The behavior is unusual, as the structure is a special class of tensegrity systems; although primarily supported by large cable (i.e., tensile) forces, the system can lose its stability due to the presence of compressed columns. The global buckling phenomenon is studied on a Geiger-type cable dome by excluding other possible buckling and failure modes. The developed numerical model, although being simple in terms of the applied elements, can consider (very) large displacements, and with the implementation of the arc-length method – with bifurcation identification and the branch switching algorithm – provides a robust solver for the analysis of general bar networks. Based on the results, the secondary load path of the Geiger cable domes is stable. This post-buckling stability (i.e., the post-critical strength reserve) is ensured by the initially inactive upper cables, which are activated after the bifurcation takes place. This phenomenon originates from the statical indeterminacy of the system. The fundamental buckling mode of the structure is a global torsional buckling, due to the small stiffness of the upper column nodes in the tangent direction of the hoops. The modified formulation of the GEVP, prescribed with the initial tangent stiffness matrix that considers the geometric stiffness of the pretension, approximates the bifurcation load level with high accuracy (a difference of less than 2%). The current paper only examined a single geometric configuration; more research on different geometries and parametric studies will be reported in the future.

Acknowledgments

This work was supported by NKFI (National Research, Development and Innovation Fund) under Grant K138615. The research reported in this paper, carried out at the Budapest University of Technology and Economics, has been supported by the Ministry for Culture and Innovation from the National Research, Development and Innovation Fund, grant number DKÖP-26-1-BME-34 (Doctoral Excellence Scholarship Program).

References

Pellegrino. S., Calladine. C.R. (1986). “Matrix Analysis of Statically and Kinematically Indeterminate Frameworks." *International Journal of Solids and Structures*, 22 (4) 409-428.

Pellegrino. S. (1990). “Analysis of Prestressed Mechanisms.” *International Journal of Solids and Structures* 26 (12) 1329-1350.

Calladine. C.R., Pellegrino. S. (1991) "First-order Infinitesimal Mechanisms." *International Journal of Solids and Structures*, 27 (4) 505-515.

Ahmed. E.A, Damatty. A.A.E (2025). "A comparative study on the stability of double-curvature and conventional cable domes." *Thin-Walled Structures* 210. 113041.

Crisfield M. (1981). "A fast incremental/iterative solution procedure that handles “snap-through”." *Computers and Structures* 13 (1-3). 55-62

Yuan. X.F., Dong. S.L. (2003) "Integral Feasible Prestress of Cable Domes." *Computers and Structures* 81. 2111-2119.

Pellegrino. S. (1992). “A class of tensegrity domes.” *International Journal of Space Structures* 7 (2). 127–142.

Rosa. R.J., Hincz. K. (2023) “Parametric analysis of a Geiger cable dome.” (In Hungarian). *Építés – Építészettudomány* 51 (3-4). 367-396.

Zhu. M.L., Dong. S.L., Yuan. X.F. (2016) “Failure Analysis of a Cable Dome Due to Cable Slack or Rupture.” *Advances in Structural Engineering* 16(2). 259-271.

Tomka P. (1997) "Lateral Stability of Cable Structures." *International Journal of Space Structures* 12 (1). 19-27.